ASME Paper Title: Optimal Design of Maxwell-Viscous Coulomb Air Damper with a Modified Fixed Point Theory

Authors: Wai On Wong, Chun Nam Wong

ASME Journal Title: Journal of Vibration and Acoustics

Volume/Issue 143/3 . Date of Publication (VOR* Online) Oct. 5, 2020 .

ASME Digital Collection URL: https://asmedigitalcollection.asme.org/vibrationacoustics/article/143/3/031002/1086 Design-of-Maxwell-Viscous-Coulomb-Air

DOI: https://doi.org/10.1115/1.4048388

The following publication Wong, W. O., & Wong, C. N. (2021). Optimal Design of Maxwell-Viscous Coulomb Air Damper With a Modified Fixed Point Theory. Journal of Vibration and Acoustics, 143(3), 031002 is available at https://doi.org/10.1115/1.4048388

Title:

Optimal Design of Maxwell-Viscous Coulomb Air Damper with a Modified Fixed Point Theory

Authors & Affiliations:

Wai On Wong[1]
Associate Professor
Email: mmwowong@polyu.edu.hk
Phone: +852-2766 6667

Chun Nam Wong[1]*
Research Associate
Email: wong.cn@yahoo.com
Phone: +852-6553 4015

[1]Department of Mechanical Engineering
The Hong Kong Polytechnic University
Hung Hom, Kowloon
Hong Kong, China

*** Corresponding Author:**

Chun Nam Wong
Research Associate
Department of Mechanical Engineering
The Hong Kong Polytechnic University
Hung Hom, Kowloon
Hong Kong, China
Phone: +852-6553 4015
Email: wong.cn@yahoo.com

Abstract

Air damper DVA is modeled using Maxwell transformed element and coulomb element. This damper serves to minimize vibration at resonant and operation of constant speed machine. Its stiffness and damping factor are transformed from Maxwell to Voigt arrangement. Meanwhile viscous equivalent Coulomb damping is expressed by absolute relative motion. System transmissibility contours are plotted by min-max approach. Its optimal parameters are determined using this approach. Contour operation minimization is obtained from minimum system transmissibility. Moreover exact solution of fixed points and optimal natural frequency ratio are obtained by a modified fixed point theory. Optimal design curve is derived by Coulomb damping derivative and maximum condition. Operational vibration level is minimized by 7% at the operation minimization using minimum condition. On the experimental side, test platform of the air damper is constructed using linear slide block system. Computational model of the air damper is established by its physical details and experimental data. Linear relationship is obtained between viscous and Coulomb damping angles. Modified fixed points are validated by frequency response function resonant peaks. Experimental vibration level is minimized by 5% which being close to the minimization result. The model is validated within 5% accuracy by its optimal experimental curve.

Keywords

air damper, Maxwell-VC DVA, Coulomb damping derivative, optimal design curve, operation minimization, linear slide block test platform

1 Introduction

Air dampers are widely used in transport industries suchas railway, motor and electric vehicles. Compared with other damper types i.e. oil and magnetic dampers, air dampers are not dependent on temperature, less maintenance works and lower production costs. On the other hand, manufacturing and construction may require higher precision works. In their designs, these are essential needs for tuning their damper elements to achieve various requirements. One of the most critical requirements is minimization of operation vibration.

For the damper arrangement, traditional models were of Voigt type in which air spring and dashpot being arranged in parallel. Three-element dynamic vibration absorber (DVA) [1-4] contained two spring elements in which one was connected to a viscous element in series and the other was placed in parallel. In its optimal design, exact solution was not easy to be obtained. In reality, spring constant and damping coefficient varies with the frequency. Also, they interact with each other and cannot be tuned independently. Main reason being that the dashpot interacts in series with the air spring. Thus the actual locations of the damping and restoring forces interaction are better described by series arrangement, such as that analysed by Asaim and Nishihara [5]. In work of Anha et al.[6], three-element DVA was attached to the damped primary structure. Four-element hybrid air damper is constructed in our model consisting of mechanical spring, Coulomb, and Maxwell elements. Air spring element is connected in series with viscous element inside the Maxwell air cylinder.

In the damping terms of the damper, Hatada et al. [7] made use of separate element force components to obtain the equations of motion. The damping term was generalized to arbitrary exponential coefficients. Mathematical model was set up for three viscous and stiffness elements only. Hydraulic actuator was used in lathe damper experiment. Moreover only viscous fluid damper was employed in their model. Third-order differential equation was established and solved by discrete time and numerical method. In its application, viscous damper with brace was mounted on building frame to reduce vibrations during strong disturbances like earthquakes. In the research of Love and Tait[8], peak factors for nonlinear DVAs as function of the number of system cycles for several power-law damping exponents. Statistical linearization was employed to represent the nonlinear damping as amplitude-dependent viscous damping and predicted the rms system response. Krenk [9] made use of dynamic amplification analysis and identification of the locus of the complex to identify damping properties of the viscous tuned mass damper natural frequencies. He analysed the dynamic amplification of the motion of the structural mass and the relative motion of the damper mass to identify the optimal damping. Bhattacharyya et al.[10] developed mathematical model of the sealed TLCD considering the pressure-volume relation in the sealed air column as an isentropic process. The effect of linearization of the air spring stiffness on damper performance was examined and found to be acceptable under certain conditions. In our paper, air spring damping is viscous with constant damping ratio. It becomes frequency dependent by transformation of series to parallel arrangement without linearization. Meanwhile air spring stiffness remains constant.

Considering the computational solution of the model, an analytical approximate constitutive relation was derived by Makris et al. [11] for a form of fluid damper which exhibited viscoelastic behavior only. The damper was used for vibration isolation of piping systems and industrial equipment, as well as for vibration and seismic isolation of building structures. In the work of Chen and Chai[12], closed-form solutions were derived for the simple structure. Brace stiffness and damper coefficient were related to the targeted reduction in response displacement or acceleration. Generalized model of Pawlak and Lewandowski[13] contained a number of Maxwell elements connected in parallel. The dynamic characteristics of a structure with this damper were determined as a solution to the Laplace transformed nonlinear eigenvalue problem. The solution to equations of motion in the frequency domain was obtained using the continuation method. In the analysis of Asaim and Nishihara [5], numerical solution and the approximated analytical solution were optimized. Anha et al.[6] established equivalent linearization method to replace approximately the original damped structure by an equivalent undamped one. Its optimal stiffness ratio and damping ratio are the same as classical methods[5]. Its damper natural frequency ratio varies between the classical optimal value according to the damping ratio of primary system. Meanwhile, its transmissibility curves were significantly lower. For our model, only quadratic differential equations are utilized instead of more complicated higher-order equations. Higher-order equations may represent more complex model, while their solutions being more difficult to obtain. Closed-form solutions of our quadratic equations are precise and obtainable in frequency domain which being more simple to analyse than those in time domains.

In the experimental aspect of Lu et al.[14], the fluid damper model was in effect same as our air damper. However, not the same as our model for which the excitation force was transmitted through structural spring to the structure. In their model, fluid damper transmited excitation force directly to the structure. SDOF quarter-car vehicle suspension system was developed by Todkar[15]. In his air damper model, viscous damper was installed in parallel connection. Air damper of cylinder-piston type and air-tank system were used in the experiment. Semi-active friction damper (SAFD) was employed by Lu et al.[16] for the seismic protection of structural systems. The LCFD system combines a traditional passive friction damper and leverage mechanism with movable central pivot. By simply controlling the pivot position, the damping force generated by the LCFD system can be adjusted in real time. Our Coulomb damping device is of rotational screw type. Damping ratio varies directly with the rotational angle. It processes tunable properties so that advanced design requirements like operation vibration minimization becoming possible.

2 System Modeling of Structural System with Maxwell-VC DVA

Schematic model of the actual air damper is shown in Fig.1. It is composed of a Coulomb element and a Maxwell viscous element (Maxwell-VC) as illustrated in Fig.2. By transforming its Maxwell element into a Voigt element, the analytical model is represented in Fig.3. Its equivalent stiffness [5] is formulated as

$$k_v = \frac{(C_m \omega)^2 k_m}{k_m^2 + (C_m \omega)^2} \tag{1}$$

with viscous damping factor C_m, spring stiffness k_m and forced frequency ω. Meanwhile, its equivalent damping factor [5] is

$$C_v = \frac{k_m^2 C_m}{k_m^2 + (C_m \omega)^2} \tag{2}$$

Using the transformed model, we can balance the forces acting on the structural system mass M and damper mass m_d to establish its equations of motion (E.O.M.s) in frequency form:

$$-MU\omega^2 + i\omega\left(C_e + C_v\right)\left(U - U_d\right) + K\left(U - V\right) + \left(k_d + k_v\right)\left(U - U_d\right) = 0 \tag{3}$$

$$-m_d U_d \omega^2 + i\omega\left(C_e + C_v\right)\left(U_d - U\right) + \left(k_d + k_v\right)\left(U_d - U\right) = 0 \tag{4}$$

where C_v is viscous damping factor, C_e is the equivalent Coulomb damping expressed by relative motion as

$$C_e = \frac{4\upsilon\Im_e}{\pi\omega\left|U_d - U\right|} \tag{5}$$

in which υ is Coulomb friction coefficient, $\Im_e$ is the normal force. Rewriting Eqs.(1,2) into matrix equation as

$$\begin{bmatrix} -M\omega^2 + K + k_d + k_v + i\omega\left(C_e + C_v\right) & -\left(k_d + k_v\right) - i\omega\left(C_e + C_v\right) \\ -\left(k_d + k_v\right) - i\omega\left(C_e + C_v\right) & -m_d\omega^2 + k_d + k_v + i\omega\left(C_e + C_v\right) \end{bmatrix} \begin{Bmatrix} U \\ U_d \end{Bmatrix} = \begin{Bmatrix} KV \\ 0 \end{Bmatrix} \tag{6}$$

Motion amplitude of M is obtained as

$$U = \frac{\left[k_d + k_v - m_d\omega^2 + i\omega\left(C_e + C_v\right)\right]KV}{\left(K + k_d + k_v - M\omega^2\right)\left(k_d + k_v - m_d\omega^2\right) - \left(k_d + k_v\right)^2 + \left[K - \left(M + m_d\right)\omega^2\right]i\omega\left(C_e + C_v\right)} \tag{7}$$

Meanwhile, amplitude of m_d can be represented by

$$U_d = \frac{\left[k_d + k_v + i\omega\left(C_e + C_v\right)\right]KV}{\left(K + k_d + k_v - M\omega^2\right)\left(k_d + k_v - m\omega^2\right) - \left(k_d + k_v\right)^2 + \left[K - \left(M + m_d\right)\omega^2\right]i\omega\left(C_e + C_v\right)} \tag{8}$$

Now, we are going to derivate the transmissibility of the system. By Eq.(6), one can get

$$\frac{U^2}{V^2}=\frac{K^2\left(k_d+k_v-m_d\omega^2\right)^2+K^2\omega^2\left(C_e+C_v\right)^2}{\left[\left(K+k_d+k_v-M\omega^2\right)\left(k_d+k_v-m_d\omega^2\right)-\left(k_d+k_v\right)^2\right]^2+\left[K-\left(M+m_d\right)\omega^2\right]^2\omega^2\left(C_e+C_v\right)^2} \tag{9}$$

Substituting Eq.(5) into Eq.(9), one can get

$$\frac{U^2}{V^2}=\frac{K^2\left(k_d+k_v-m_d\omega^2\right)^2\pi^2\omega^2\left|U_d-U\right|^2+K^2\omega^2\left(4\upsilon\Im_e+C_v\pi\omega\left|U_d-U\right|\right)^2}{\begin{array}{l}\left[\left(K+k_d+k_v-M\omega^2\right)\left(k_d+k_v-m_d\omega^2\right)-\left(k_d+k_v\right)^2\right]^2\pi^2\omega^2\left|U_d-U\right|^2\\ +\left[K-\left(M+m_d\right)\omega^2\right]^2\omega^2\left(\left(4\upsilon\Im_e+C_v\pi\omega\left|U_d-U\right|\right)\right)^2\end{array}} \tag{10}$$

Relative motion between U_d and U is computed by Eqs.(6,7),

$$\begin{aligned}&\pi^2 m_d\omega^2\Im_e^2=\\&\left[\left(K+k_d+k_v-M\omega^2\right)\left(k_d+k_v-m_d\omega^2\right)-\left(k_d+k_v\right)^2\right]^2\pi^2\omega^2\left|U_d-U\right|^2\\&+\left[K-\left(M+m_d\right)\omega^2\right]^2\omega^2\left(\left(4\upsilon\Im_e+C_v\pi\omega\left|U_d-U\right|\right)\right)^2\end{aligned} \tag{11}$$

By expressing this equation in quadratic non-dimensional form, one arrives at

$$\begin{aligned}&\left\{\mu^2\pi^2\left[\left(1+\mu\gamma_d^2+\frac{\mu\lambda^2\varsigma_m^3\gamma_m^2}{1+\lambda^2\varsigma_m^2}-\lambda^2\right)\left(\gamma_d^2+\frac{\lambda^2\varsigma_m^3\gamma_m^2}{1+\lambda^2\varsigma_m^2}-\lambda^2\right)-\frac{1}{\mu}\left(\mu\gamma_d^2+\frac{\mu\lambda^2\varsigma_m^3\gamma_m^2}{1+\lambda^2\varsigma_m^2}\right)^2\right]^2\right.\\&\left.+4\pi^2\left[1-\left(1+\mu\right)\lambda^2\right]^2\left(\gamma_d^2+\frac{\lambda^2\varsigma_m^3\gamma_m^2}{1+\lambda^2\varsigma_m^2}\right)^2\right\}\left|\frac{U_d-U}{V}\right|^2\\&+16\upsilon f\pi\frac{\mu\lambda^2\varsigma_m^3\gamma_m^2}{1+\lambda^2\varsigma_m^2}\left[1-\left(1+\mu\right)\lambda^2\right]^2\left|\frac{U_d-U}{V}\right|+16\upsilon^2f^2\left[1-\left(1+\mu\right)\lambda^2\right]^2-\pi^2\lambda^4\mu^2=0\end{aligned} \tag{12}$$

where $\mu=\frac{m_d}{M}$ is the mass ratio, $\omega_d=\sqrt{k_d/m_d}$ is the natural frequency of DVA, $\omega_m=\sqrt{k_m/m_d}$ is the natural frequency of viscous element, $\omega_n=\sqrt{K/M}$ is the natural frequency of structural system, $\varsigma_m=C_m\omega_n/k_m$ is viscous damping ratio, $\gamma_d=\omega_d/\omega_n$ is DVA natural frequency ratio, $\gamma_m=\omega_m/\omega_n$ is viscous damper natural frequency ratio,

$\lambda = \omega/\omega_n$ is the forced frequency ratio, $f = \Im_e/KV$ is the force ratio. Solving this equation to obtain the explicit solution of the transmissibility of relative motion,

$$\left|H(U_d - U)\right| = \left|\frac{U_d - U}{V}\right| = \left|\frac{-U_2 \pm \sqrt{U_2^2 - 4U_1U_3}}{2U_1}\right| = \frac{|U_4|}{|U_1|} \tag{13}$$

where

$$U_1 = \mu^2\pi^2\left[\left(1+\mu\gamma_d^2 + \frac{\mu\lambda^2\varsigma_m^3\gamma_m^2}{1+\lambda^2\varsigma_m^2} - \lambda^2\right)\left(\gamma_d^2 + \frac{\lambda^2\varsigma_m^3\gamma_m^2}{1+\lambda^2\varsigma_m^2} - \lambda^2\right) - \frac{1}{\mu}\left(\mu\gamma_d^2 + \frac{\mu\lambda^2\varsigma_m^3\gamma_m^2}{1+\lambda^2\varsigma_m^2}\right)^2\right]^2$$

$$+4\pi^2\left[1-(1+\mu)\lambda^2\right]^2\left(\gamma_d^2 + \frac{\lambda^2\varsigma_m^3\gamma_m^2}{1+\lambda^2\varsigma_m^2}\right)^2$$

$$U_2 = 16\upsilon f\pi\frac{\mu\lambda^2\varsigma_m^3\gamma_m^2}{1+\lambda^2\varsigma_m^2}\left[1-(1+\mu)\lambda^2\right]^2$$

$$U_3 = 16\upsilon^2 f^2\left[1-(1+\mu)\lambda^2\right]^2 - \pi^2\lambda^4\mu^2$$

$$U_4 = \frac{-U_2 \pm \sqrt{U_2^2 - 4U_1U_3}}{2}$$

$$\varsigma_c = \upsilon f$$

Using this solution in the non-dimensionalized Eq.(8),

$$H^2(U) = \frac{\mu^2\left(\gamma_d^2 + \frac{\lambda^2\varsigma_m^3\gamma_m^2}{1+\lambda^2\varsigma_m^2} - \lambda^2\right)^2\pi^2|U_4|^2 + \left(4\varsigma_c|U_1| + \frac{2\pi\mu\lambda^2\varsigma_m^3\gamma_m^2}{1+\lambda^2\varsigma_m^2}|U_4|\right)^2}{\mu^2\left[\left(1+\mu\gamma_d^2 + \frac{\mu\lambda^2\varsigma_m^3\gamma_m^2}{1+\lambda^2\varsigma_m^2} - \lambda^2\right)\left(\gamma_d^2 + \frac{\lambda^2\varsigma_m^3\gamma_m^2}{1+\lambda^2\varsigma_m^2} - \lambda^2\right) - \frac{1}{\mu}\left(\mu\gamma_d^2 + \frac{\mu\lambda^2\varsigma_m^3\gamma_m^2}{1+\lambda^2\varsigma_m^2}\right)^2\right]^2\pi^2|U_4|^2 + \left[1-(1+\mu)\lambda^2\right]^2\left(4\varsigma_c|U_1| + \frac{2\pi\mu\lambda^2\varsigma_m^3\gamma_m^2}{1+\lambda^2\varsigma_m^2}|U_4|\right)^2}$$

(14)

By Eq.(13), its system transmissibility is reduced to

$$\left|H\left(U\right)\right|=\frac{\left|\sqrt{\left(\gamma_d^2+\frac{\lambda^2\varsigma_m^3\gamma_m^2}{1+\lambda^2\varsigma_m^2}-\lambda^2\right)^2+\left(4\varsigma_c/\pi\mu\left|H\left(U_d-U\right)\right|+\frac{2\lambda^2\varsigma_m^3\gamma_m^2}{1+\lambda^2\varsigma_m^2}\right)^2}\right|}{\left|\sqrt{\begin{array}{l}\left[\left(1+\mu\gamma_d^2+\frac{\mu\lambda^2\varsigma_m^3\gamma_m^2}{1+\lambda^2\varsigma_m^2}-\lambda^2\right)\left(\gamma_d^2+\frac{\lambda^2\varsigma_m^3\gamma_m^2}{1+\lambda^2\varsigma_m^2}-\lambda^2\right)-\mu\left(\gamma_d^2+\frac{\lambda^2\varsigma_m^3\gamma_m^2}{1+\lambda^2\varsigma_m^2}\right)^2\right]^2\\+\left[1-\left(1+\mu\right)\lambda^2\right]^2\left(4\varsigma_c/\pi\mu\left|H\left(U_d-U\right)\right|+\frac{2\lambda^2\varsigma_m^3\gamma_m^2}{1+\lambda^2\varsigma_m^2}\right)^2\end{array}}\right|} \quad (15)$$

3 Contour Plots using Min-Max Approach

3.1 Maximum system transmissibility to determine contour optimal.

From practical experience, one makes use of the mass ratio $\mu=0.2$ and $\gamma_d=\frac{1}{1+\mu}=$ 0.8333. Same result was reported by Krenk[9] where only constant spring stiffness and viscous damping element being used. Its stiffness ratio $K_r=\frac{k_m}{k_d}$ can be optimal tuned near $\gamma_m=10\gamma_d$, i.e. $K_r=\sqrt{10}=3.16$. Sequential tuning are carried out on the optimal damping ratios, ς_m and ς_c. For the γ_d, successive half reductions of 20% tuning range are applied at its transmissibility curves. After five tunings, its optimal value is obtained as $\gamma_d^{'}$ = 0.8073 with 3.12% decrement. Similarly, optimal $\gamma_m^{'}$ is obtained to be 8.125 after three tunings with 2.50% decrement. From one of its tuning, its range is set to be $[0.9\gamma_m^{'}, 1.1\gamma_m^{'}]$ in $0.1\gamma_m^{'}$ interval. From its curves, only two fixed points are observed at $\lambda_{P,Q}^{'}$ = 0.75, 1.02 respectively. This agrees with the quadratic form of fixed points frequency equation. Subsequently, viscous and Coulomb damping ratio plane is used in contour plots. Contour chart of ranges ς_m =

[0.09,0.13] and ς_c= [0.10,0.25] is illustrated in Fig.4. It appears as valley shaped optimal zone embedded by curved contour lines using min(max$|H(U)|$) approach. The most inner contour is 3.4 level, where the optimal value is 3.325 (W) at ς_m= 0.10 and ς_c= 0.22. From its transmissibility curve (Fig.5), two resonant peaks are identified at $\lambda'_{P,Q}$= 0.78, 1.08. The corresponding $|H(U)|_{\lambda'_{P,Q}}$ = 3.325, 3.162. As their difference is only 5.16%, the equal transmissibility at global optimal is validated. Three-element model of Asaim and Nishihara [5] is compared with our Maxwell model for further validation. Its system transmissibility is listed as

$$|H(U)| = \left| \sqrt{\frac{K_r^2\gamma_d^2\left(\gamma_d^2-\lambda^2\right)^2+4\varsigma^2\lambda^2\left((1+K_r)\gamma_d^2-\lambda^2\right)^2}{\begin{array}{l}K_r^2\gamma_d^2\left(\gamma_d^2-\left(1+(1+\mu)\gamma_d^2\right)\lambda^2+\lambda^4\right)^2+\\4\varsigma^2\lambda^2\left\{(1+K_r)\gamma_d^2-\left[1+(1+\mu)(1+K_r)\gamma_d^2\right]\lambda^2+\lambda^4\right\}^2\end{array}}} \right| \qquad (16)$$

Their model is optimized by $\gamma_d = \sqrt{\frac{1}{1+\mu}\left(1-\sqrt{\frac{\mu}{1+\mu}}\right)}$ = 0.702, $\gamma_m = \gamma_d K_{rOpt}$ = 0.9689, $K_{rOpt} = 2\left[\mu+\sqrt{\mu(1+\mu)}\right]$ = 1.380, $\varsigma = \frac{\varsigma_m\gamma_d K_r}{4}$, $\varsigma_{Opt} = \sqrt{\frac{1+r}{r}\cdot\frac{-b-\sqrt{b^2-ac}}{a}}$ = 0.3685 where $r = \sqrt{\frac{1+\mu}{\mu}}$ = 2.450, $a = -2-2r+5r^2+4r^3-2r^5+r^6$ = 121.5, $b = 2-3r^2-r^4$ = -52.0, $c = -2+2r+r^2$= 8.899. Transmissibility curve of its contour optimal is plotted in Fig.5. The resonant peaks are obtained at $\lambda''_{P,Q}$= 0.76, 1.14 for which their differences are only 2.63% and 5.56% respectively from the developed model. As its fixed points frequency ratio equation is in third-order, there are three fixed points. However, they not located at the resonant peaks and on their 74% levels. For Krenk'[9] work, fixed optimal stiffness ratio

$K_{rOpt}^{K} = 2\left[\mu + \sqrt{\mu(1+\mu)}\right]$ = 1.380 is the same. Its $\varsigma_{Opt} = \sqrt{\mu/2(1+\mu)}$ =0.2887 is 21% reduced from ς_{Opt}. Only optimal solution is obtained from his model which being non-tunable.

3.2 Minimum system transmissibility to determine contour minimization.

Assume that system operation frequency ratio λ_s ranges between 3 to 7. In order to check up the minimum vibration level at λ_s= 3, $\min|H(U)|$ contour is plotted in Fig.6. The contour becomes straight line of 0.103 level where operation minimization line of ς_c= 0.14 is obtained across the whole range of ς_m. This operation minimization value is significantly reduced 36.4% from that at W. Thus this level is pre-set during the design process. Above this level, they increase concave upward from 0.103 to 0.112 level. Meanwhile, below this minimization level, they increase from 0.103 to 0.113 level as slandered lines. This is indicated by X on Fig.6.

Now suppose that the operation frequency increase to the higher limit at which λ_s becomes 7. From its contour minimization in Fig.6, the Coulomb damping ratio is 0.13. Along the Maxwell optimal curve, minimum search is carried out to match up this requirement. Ultimately, the minimization viscous damping ratio is attained at Y in Fig.6 where ς_m= 0.112. At this minimization setting, ς_m is slightly increased 12% from ς_m= 0.10. Utilizing this minimization setting, its transmissibility curve is plotted in Fig.5. Minimization is effective over nearly the whole frequency ratio range except at the range near λ_s= 1.4 induced by the optimal Coulomb damping ratio. It is enhanced from contour optimal value of 0.0187 to 0.0174 accounting for 6.93% vibration minimization. Comparing with the three-element model in Fig.5, no minimization is induced near $\lambda_s = 1.4$. Its optimal vibration level at $\lambda_s = 7$ is 0.0209 with 11.8% increment from contour optimal. With the addition of Coulomb element, the model can be tuned at different parameters such as K_r. This brings down the vibration levels substantially at various ranges above.

4 Optimal Resonant by Modified Fixed Point Theory

4.1 Exact solution of fixed points and optimal natural frequency ratio.

In order to compute the exact solutions of the fixed points *P* and *Q*, one can make use of the cases where $\varsigma_c, \varsigma_m = 0$ and $\varsigma_c, \varsigma_m = \infty$. For the first case, we have

$$H(U) = \frac{\gamma^2 - \lambda^2}{\left(1 + \mu\gamma^2 - \lambda^2\right)\left(\gamma^2 - \lambda^2\right) - \mu\gamma^4} \tag{17}$$

For the second case, when $\varsigma_c, \varsigma_m = \infty$

$$H(U) = \frac{1}{1 - (1+\mu)\lambda^2} \tag{18}$$

As the two fixed points must pass through these two spectra, one equals them in opposite phases

$$\frac{\gamma^2 - \lambda^2}{\left(1 + \mu\gamma^2 - \lambda^2\right)\left(\gamma^2 - \lambda^2\right) - \mu\gamma^4} = \frac{-1}{1 - (1+\mu)\lambda^2} \tag{19}$$

Simplifying this equation, the frequency ratio equation is obtained as

$$(2+\mu)\lambda^4 - 2\left[1 + (1+\mu)\gamma^2\right]\lambda^2 + 2\gamma^2 = 0 \tag{20}$$

This is a quadratic equation with two distinct real roots solved by

$$\lambda_P^2 = \frac{1+(1+\mu)\gamma^2 - \sqrt{1-2\gamma^2+(1+\mu)^2\gamma^4}}{2+\mu} \tag{21}$$

and

$$\lambda_Q^2 = \frac{1+(1+\mu)\gamma^2 + \sqrt{1-2\gamma^2+(1+\mu)^2\gamma^4}}{2+\mu} \tag{22}$$

Substituting $\lambda_{P,Q}$ back to Eq.(18) and equating $\left|H\left(\lambda_P\right)\right| = -\left|H\left(\lambda_Q\right)\right|$, we have

$$\frac{1}{1-(1+\mu)\lambda_P^2} = \frac{-1}{1-(1+\mu)\lambda_Q^2} \tag{23}$$

which can be expressed as

$$\lambda_P^2 + \lambda_Q^2 = \frac{2}{1+\mu} \tag{24}$$

From the frequency ratio equation, the sum of roots is

$$\lambda_P^2 + \lambda_Q^2 = \frac{1+(1+\mu)\gamma_{dOpt}^2}{2+\mu} \tag{25}$$

Equating Eqs.(23,24), both frequency ratios are eliminated at the same time. Thus one can get the optimal gamma as

$$\gamma_{dOpt} = \frac{1}{1+\mu} \tag{26}$$

Hence this assumption in the contour analysis is validated. Similar approach is used by Wong and Cheung[17] in their derivation of optimal gamma. Substituting γ_{dOpt} to Eqs.(20,21), the optimal frequency ratios at the fixed points are

$$\lambda_P^2 = \frac{\sqrt{2+\mu}-\sqrt{\mu}}{(1+\mu)\sqrt{2+\mu}} \tag{27}$$

$$\lambda_Q^2 = \frac{\sqrt{2+\mu}+\sqrt{\mu}}{(1+\mu)\sqrt{2+\mu}} \tag{28}$$

When the optimal μ takes the value of $\mu_{dOpt} = 0.2$, using Eq.(26) the optimal value of γ_{dOpt} is 0.8333 which is deviated 3.12% from $\gamma_d^{'}$ in contour analysis. The frequency ratios are λ_P = 0.7629 and λ_Q = 1.0414 at fixed points P and Q. Their percentage errors from contour optimal in previous section are 2.24% and 3.71% only. Substituting these optimal parameters into Eq.(18), one obtains the optimal $|H(U)|$ at λ_P,

$$H(U)\big|_{\lambda_P} = \frac{1}{1-(1+\mu)\dfrac{\sqrt{2+\mu}-\sqrt{\mu}}{(1+\mu)\sqrt{2+\mu}}} \tag{29}$$

Considering its absolute value, it is reduced to

$$|H(U)|_{\lambda_P} = \sqrt{\frac{2+\mu}{\mu}} \tag{30}$$

Meanwhile for the second fixed point λ_Q, using optimal parameters in Eq.(18) one gets

$$H(U)\big|_{\lambda_Q} = \frac{1}{1-(1+\mu)\dfrac{\sqrt{2+\mu}+\sqrt{\mu}}{(1+\mu)\sqrt{2+\mu}}} \tag{31}$$

Then its absolute value is

$$\left|H(U)\right|_{\lambda_Q} = \sqrt{\frac{2+\mu}{\mu}} \tag{32}$$

Notice that Eqs.(30,32) are the same, proving that transmissibilities at both fixed points are at equal level. For the Asami's air damper model, resonant peak $\left|H(U)\right|_{\max} = \sqrt{2/\mu} = 3.162$. Its percentage error is 4.65% from $\left|H(U)\right|_{\lambda_{P,Q}} = 3.317$. Therefore these theoretical fixed points are right at the resonant peaks. The analysis from Krenk[9] is the same as $\left|H(U)\right|^{K}_{\lambda_{P,Q}} = \sqrt{\frac{2+\mu}{\mu}} = 3.317$.

4.2 Coulomb damping derivative to derive optimal design curve.

Consequent step is to determine the optimal design curve using optimal damping ratios. The full expression of Eq.(14) is used in the next computation. Not the same as traditional approach, we make use of Coulomb damping derivative of this transmissibility. From the contour plot, the optimal zone varies as higher-order curves in ς_c and ς_m. Putting a cross-section at each fixed ς_c, ς_m varies in valley shaped curve. In general, there is a minimum at the bottom of this curve. At this minimum level, they become the stationary points, such that

$$\frac{\partial H^2(U)}{\partial \varsigma_m} = \frac{\left(C^2 + D^2B^2\right)2BB' - \left(A^2 + B^2\right)2D^2BB'}{\left(C^2 + D^2B^2\right)^2} = 0 \tag{33}$$

where $A = \gamma_d^2 + \frac{\lambda^2 \varsigma_m^3 \gamma_m^2}{1+\lambda^2\varsigma_m^2} - \lambda^2$, $B = 4\varsigma_c / \pi\mu \left|H(U_d - U)\right| + \frac{2\lambda^2 \varsigma_m^3 \gamma_m^2}{1+\lambda^2\varsigma_m^2}$,

$$C = \left(1 + \mu\gamma_d^2 + \frac{\mu\lambda^2\varsigma_m^3\gamma_m^2}{1+\lambda^2\varsigma_m^2} - \lambda^2\right)\left(\gamma_d^2 + \frac{\lambda^2\varsigma_m^3\gamma_m^2}{1+\lambda^2\varsigma_m^2} - \lambda^2\right) - \mu\left(\gamma_d^2 + \frac{\lambda^2\varsigma_m^3\gamma_m^2}{1+\lambda^2\varsigma_m^2}\right)^2,$$

$$D = 1 - (1+\mu)\lambda^2$$

By simplifying Eq.(33) as

$$\left(C^2 - A^2 D^2\right) 2BB' = 0 \tag{34}$$

optimal damping conditions can be obtained. There are three essential components in this equation, namely, damping component B, its derivative B' and optimal parameter component $C^2 - A^2D^2$. Notice that $C^2 - A^2D^2$ is a function of optimal parameters except the damping ratios. Therefore, it can be listed as non-zero constant. In order to satisfy Eq.(34), at least one of the two components must be at zero value. Considering different conditions of component B', when $B' \neq 0$, let $B' = c$, one can integrate it to get a one order higher component $B = f(\varsigma_c)$. Thus both B and B' are non-zero, and condition of Eq.(34) is not satisfied. When $B' = 0$, we can obtain $B = c$ by integration which is a non-zero component. Hence the optimal damping condition is satisfied. For the first condition, it gives

$$B' = \frac{4\mu\pi\left|H(U_d - U)\right| - 4\varsigma_c \pi\mu \,\partial H(U_d - U)/\partial \varsigma_c}{\mu^2\pi^2\left|H(U_d - U)\right|^2} = 0 \tag{35}$$

The Coulomb damping ratio is computed from this equation as

$$\varsigma_c = \frac{\left|H(U_d - U)\right|}{\partial\left|H(U_d - U)\right|/\partial\varsigma_c} \tag{36}$$

From the second condition, its equation is established as

$$B = 4\varsigma_c/\pi\mu\left|H(U_d - U)\right| + \frac{2\lambda^2\varsigma_m^3\gamma_m^2}{1+\lambda^2\varsigma_m^2} = c_C \tag{37}$$

To obtain the unique optimal curve, the arithmetic means of specific coefficients in Eq.(37) are used. Its equation can be expressed in fixed points solution as

$$\varsigma_{cOpt} = C_C - \frac{\varsigma_{mC}\varsigma_m^3}{2\left(1+\lambda_C^2\varsigma_m^2\right)} \tag{38}$$

in which $C_C = \frac{C_P + C_Q}{2}$ where $C_{P,Q} = \frac{\mu\pi\left|H\left(U_d - U\right)\right|_{P,Q} c_C}{4}$, $\varsigma_{mC} = \frac{\varsigma_{mP} + \varsigma_{mQ}}{2}$ where $\varsigma_{mP,Q} = \mu\pi\left|H\left(U_d - U\right)\right|_{P,Q}\lambda_{P,Q}^2\gamma_m^2$, $\lambda_C^2 = \frac{\lambda_P^2 + \lambda_Q^2}{2}$. Besides ς_c and ς_m , other terms in Eq.(38) are considered to be invariant. Thus it is a third-order curve of optimal damping ratios. At the optimal condition, $\left|H\left(U_d - U\right)\right|$ becomes maximum. Using Eq.(13), its U_4 attains the maximum value when $U_4 = \frac{-U_2 - \sqrt{U_2^2 - 4U_1U_3}}{2} = -U_2$, i.e. $4U_1U_3 = 0$. This condition is obtained when either $U_1 = 0$ or $U_3 = 0$. One can observe that U_1 contains ς_m as variant only under the optimal condition. Substituting the optimal parameters in previous section into U_1, the fixed points ς_m are obtained. Their arithmetic mean is $\varsigma_{mOpt} = 0.00296$. Similarly, U_3 contains ς_c as the only variant under the optimal condition. $U_3 = 0$ is the correct equation to obtain the optimal value of ς_{cOpt}. Using the optimal parameters in previous section to solve this optimal condition, the fixed points ς_c are obtained. ς_{cOpt} is computed as 0.388 by their arithmetic mean. As $\left[\varsigma_c, \varsigma_m\right]_U$ = [0.388, 0.00296] is close to the intercept point, one obtains $C_C = \varsigma_{cOpt}$. Using its definition in Eq.(38), the optimal value of c_C is determined to be 0.36. Substituting the optimal parameters of μ', γ_{dOpt}, $K_r^{'}$, $\lambda_{P,Q}$, ς_{cOpt}, ς_{mOpt} into Eq.(38), the optimal design curve is plotted in Fig.7. Compared with contour optimal, larger percentage errors are 2.22% and 7.38% around ς_m = 0.08 and 0.10. To analyse the deviation along the whole curve, mean absolute deviation ratio is used as

$$\overline{E\left(\varsigma_c\right)} = \sum_{i=1}^{n} \left| \left(\varsigma_{cEi} - \varsigma_{cOpti}\right) \middle/ \varsigma_{cOpti} \right| \Big/ n \tag{39}$$

which is calculated to be $\overline{E\left(\varsigma_c\right)}$ = 0.092. Using contour chart of max$\left|H\left(U_d - U\right)\right|$ in Fig.8, a large portion of optimal curve follows similar contour pattern at max$\left|H\left(U_d - U\right)\right|$ = 10. Thus the invariant property of $\left|H\left(U_d - U\right)\right|$ along the optimal curve is validated.

5 Minimization of Operational Vibration Response

On the other hand, one determines the operation minimization min$\left|H(U)\right|$ at operation frequency λ_s instead of fixed points frequencies $\lambda_{P,Q}$. Not the same as the optimal curve of Eq.(38), it appears to be a straight line with nearly constant value of ς_{cs}. Instead, we make use of the first condition in Eq.(36) to seek its exact solution. One can observe that this equation contains two variables only, namely, ς_{cs} and $\left|H\left(U_d - U\right)\right|_{\lambda s}$. Thus they are rearranged separately into

$$\frac{\partial \varsigma_{cs}}{\varsigma_{cs}} = \frac{\partial \left|H\left(U_d - U\right)\right|_{\lambda s}}{\left|H\left(U_d - U\right)\right|_{\lambda s}} \tag{40}$$

Integrating this equation on both sides simultaneously, one gets its logarithmic form

$$\ln \varsigma_{cs} - \ln \varsigma_{c1} = \ln\left|H\left(U_d - U\right)\right|_{\lambda s} - \ln\left|H\left(U_d - U\right)\right|_{\lambda 1} \tag{41}$$

which is further simplified by

$$\frac{\varsigma_{cs}}{\varsigma_{c1}} = \frac{\left|H\left(U_d - U\right)\right|_{\lambda s}}{\left|H\left(U_d - U\right)\right|_{\lambda 1}} \tag{42}$$

Assume that $\left|H(U_d - U)\right|_{\lambda 1}$ becoming zero at an arbitrary ς_{c1}, we can solve ς_{c1} directly from $\left|H(U_d - U)\right|_{\lambda 1} = 0$. Substituting this back to Eq.(41), one gets $\frac{\varsigma_{cs}}{\varsigma_{c1}} = \frac{\left|H(U_d - U)\right|_{\lambda s}}{0}$. To avoid singular solution, this is rearranged as

$$\left|H(U_d - U)\right|_{\lambda 1} = \frac{0 \times \varsigma_{cs}}{\varsigma_{c1}} = 0 \qquad (43)$$

Making use of Eq.(13), this minimization equation becomes $U_4 = 0$. Equating one of its quadratic root to zero, one gets $-U_2 + \sqrt{U_2^2 - 4U_1U_3} = 0$. To solve for ς_c, the necessary condition is $U_3 = 0$. Substituting minimization parameters into this condition, one gets

$$16\varsigma_{cs}^2\left[1 - (1 + \mu')\lambda_s^2\right]^2 - \pi^2\lambda_s^4\mu'^2 = 0 \qquad (44)$$

Under invariant operation speeds λ_s, one obtains its corresponding Coulomb damping ratio as

$$\varsigma_{cs} = \frac{\pi\mu'\lambda_s^2}{4\left[(1 + \mu')\lambda_s^2 - 1\right]} \qquad (45)$$

As the operation frequency λ_s is pre-set to be 3, ς_{cs} is generated as 0.1443. Comparing with the contour minimization of ς_{cs}= 0.14, its percentage error is 0.69%. As the error is within 1% accuracy level, Eq.(44) is precise in determining the Coulomb damping ratio. As $\min\left|H(U)\right|$ is constant along this design line, the operation minimization is tuned by Coulomb damper solely. Fixed points minimization is obtained by interception of two design curves in Fig.6 at X. Comparing its $\left|H(U)\right|$ with contour minimization of 0.265, the $\min\left|H(U)\right|$ of 0.278 in Fig.5 is 4.46% reduced. Meanwhile by optimal curve in Eq.(38), minimization viscous damping ratio is generated at ς_{ms}= 0.112 with slight reduction from fixed points optimal. Therefore viscous damping ratio can be reduced by adding Coulomb damper in the DVA. From its relative transmissibility curve at Fig.9, there is a spur drop to 2.04×10^{-4} level indicated by dotted circle right at λ_s = 3. Hence the assumption of $\left|H(U_d - U)\right|_{\lambda s}$ becoming zero is validated at fixed point minimization. DVA completely separated from the machine system, no interaction between the dampers and the system. The spur shaped drop try to shift the DVA towards the operation frequency λ_s once it is deviated. This guarantees stable operation of the machine at operation frequency. Comparing Figs.7 and 8, one can observe that they follow nearly the same contour pattern at the Maxwell optimal curve. For the $\left|H(U_d - U)\right|_{\lambda s}$ contour plot, its optimal curve enter the 10 level at ς_m = 0.07. Therefore the invariant property of $\left|H(U_d - U)\right|_{P,Q}$ along the optimal design curve is validated.

Its $\left|H(U)\right|$ curve is compared with that of fixed points optimal in Fig.5. There are larger discrepancies near $\lambda_s = 0.65$ and toggled between $\lambda_s = 0.70$ during start-up. Then they are near $\lambda_s = 1.40$ and toggled between operation frequency λ_s = 3.0. Keeping only the λ_s as variant in Eq.(43), it is reduced to

$$\lambda_s = 2\sqrt{\frac{\varsigma_{cs}}{4\varsigma_{cs}(1+\mu') \pm \pi\mu'}} \qquad (46)$$

Using previous obtained ς_{cs} = 0.1443, two minimization frequency ratios, namely λ_{s1} = 3.000 and λ_{s2} = 0.661 are obtained. λ_{s1} is the original required operation frequency, while λ_{s2} is an extra frequency from minimization condition. This explains the additional minimum zone before the fixed points frequency λ_P. Using its $\left|H(U_d - U)\right|$ curve in Fig.9, one can locate the extra $\lambda_{s2} = 0.66$ inside the first range. Meanwhile λ_{s1} is suited near the second range.

On the other hand, at the contour optimal ς_c = 0.22 two minimum frequency ratios, namely λ_{s3} = 0.723 and λ_{s4} = 1.434, are obtained which rightly fit into the large discrepancy ranges. Hence the discrepancies in various λ_s are fully explained by the minimum frequency equation of Eq.(45). By continuous increment of λ_s, the Coulomb damping ratio converges to 0.131. As further increase in λ_s does not change this ς_{cs}, this becomes the termination point of optimal design curves as in Figs.7,8.

6 Experimental Validation by Linear Slide Block Platform

Test platform of vibration absorber is designed and installed for adjustable mass, spring and damping effect. Linear slide block system is established for linear horizontal motion of DVA system consisted of slide blocks, linear guide rail and support rail as demonstrated in Fig.10. Ground motion is transmitted from the shaker to the system through ground spring. Vibration signals on slide block and shaker are captured by accelerometers. These signals are conditioned at the spectrum analyser. Details of the air damper are shown in Fig.11. Using these data, damping coefficient, spring constant and coefficient of discharge resistance are computed as follows[5]. First, the damping coefficient C_m is determined by the coefficient of discharge resistance α_1, diameter and area of piston d_p, A_p, air chamber factor N_1.

$$N_1 = \frac{\alpha_1 \omega A_p h_p}{\gamma p_0} \tag{47}$$

where h_p is height from bottom of cylinder to the piston, γ is the ratio of air specific heat, ρ_0, p_0 are the atmospheric air density and pressure. Second, spring constant is computed using

$$k_m = \frac{\gamma p_0 A_p}{h_p} \tag{48}$$

Third, coefficient of discharge resistance is calculated by

$$\alpha_1 = \frac{\sqrt{\gamma p_0 \rho_0 \Im / h_p}}{b_1 \left(c_o A_o + c_d A_d\right)} \tag{49}$$

where b_1 is coefficient constant, c_o, c_d are the flow coefficients, A_o, A_d are the areas of clearance and orifice. Ultimately, viscous damping factor

$$C_m = \frac{\alpha_1 A_p^2}{N_1 \times 10^{-5}} \sqrt{\frac{\sqrt{1 + N_1^4} - 1}{2}} \tag{50}$$

Viscous damping ratio is computed by its definition $\varsigma_m = C_m \omega_n / k_m$ along the optimal design curve. Effort is tried to regulate the ς_m using measured θ_v . As $0 \le A_d \le 3.85 \times 10^{-5} m^2$ varies linearly with $0 \le \theta_v \le 120^\circ$ along the optimal experimental curve, they are related by $A_d = c_v \theta_v$ where $c_v = 3.2 \times 10^{-7}\ m^2 / \deg$ is the viscous angle factor. Its corresponding Coulomb damping ratio is calculated by $\varsigma_c = \Im_c / KV$ in which Coulomb damping force $\Im_c = \upsilon \Im_e$. As the variation of ground motion is kept low at the optimal curve, one can assume that KV to be constant. Fastening screw tuning Coulomb damping angle θ_c is related to $\Im_c$ with Coulomb angle factor c_f and residual damping force c_r , i.e. $\varsigma_c = \left(c_f \theta_c + c_r\right) / KV$. In the line fitting of Coulomb force test, c_f = 0.0178 $N / \deg$ and $c_r = 0.622 N$ from Fig.12. These two damping ratios are optimal tuned to measure the optimal $\left|H(U)\right|_{\lambda_{P,Q}}$ at each data set. The data set of these angles form the optimal curve in Fig.13. Using the spectrum analyser, frequency response functions (FRFs) at ς_c -axis intercept V_e, optimal W_e and minimization Y_e are obtained at Fig.14. Their maximum peaks are recorded in Fig.15. They drop gradually from V_e to minimum at W_e and raise to Y_e afterwards. Using Fig.14, one can observe that there is a minimization zone near λ_s = 2 caused by the induced Coulomb friction on the slide blocks. Beyond this zone, the minimization norm ratio $\left\| \left| H(U)_W \right| - \left| H(U)_Y \right| \right\| \big/ \left\| H(U)_W \right\|$ = 0.071 between λ_s = 3 to 5. Hence operation vibration level is minimized around 7%. The frequency ratios are λ_P^e = 0.80 and λ_Q^e = 1.10 at fixed points *P* and *Q*. Comparing the FRF resonant peaks with that of fixed points in Fig.6, the errors of $\lambda_{P,Q}$ are 4.86% and 6.01%. These are accurate within 7% accuracy. Meanwhile for the errors in $\left| H(U) \right|_{\lambda_{P,Q}}$, they are -3.75% and -3.32% respectively. By this relationship, the optimal experimental curve is furnished in Fig.16. On the ς_c-axis intercept, ς_{cV}^e = 0.395 which is 1.8% larger than ς_{cOpt} = 0.388. On the other hand, their percentage errors are 2.0% and 1.8% at experimental optimal ς_{mW}^e = 0.098 and minimization ς_{mY}^e = 0.110 respectively. These deviations are mainly due to the misaligned spring, non-smooth sliding motion, part clearance, induced Coulomb friction, simplified air damper model, slide block-DVA interaction, etc. To analyse the deviation along the whole curve, mean absolute deviation ratio is used as

$$\overline{E(\varsigma_c)} = \sum_{i=1}^{n} \left| \left(\varsigma_{cEi} - \varsigma_{cOpti} \right) \big/ \varsigma_{cOpti} \right| \Big/ n \tag{51}$$

which is calculated to be $\overline{E(\varsigma_c)}$ = 0.0453. As the mean deviation is within 5% accuracy, the air damper model is validated by its measured data.

7 Conclusions

Four-element hybrid DVA is constructed using Coulomb and Maxwell transformed elements. Optimal parameters of its system transmissbility are obtained using modified fixed points theory which are validated by three-element model. Two fixed points are located at the resonant peaks. Using viscous damping derivative conditions, its third-order optimal design curve deviates slightly within 8% from the contour analysis. Operation minimization is highly effective by tuning the damping elements along this design curve. Vibration level is reduced 19% from the three-element model. Its operation range is well suited between λ_s = 3 to 7 and can be extended to higher frequency ratio. By both optimal and minimization Coulomb damping ratios, four minimization zones are created to further bring down vibration levels. Test platform of the air damper is constructed. Linear relationship is obtained between θ_v and θ_c. Model fixed points are validated by FRF resonant peaks. Optimal experimental curve is computed using developed model and compared with the optimal design curve within acceptable accuracies. At operation range λ_s = 3 to 5, vibration level is effectively minimized by 5% close to the model predicted. The percentage errors of measured ς_c are within 2.0% accuracy. Using mean deviation of optimal curve, the air damper model is validated in 5% accuracy by the test platform.

Acknowledgment

The authors gratefully thank the support from Research Grant Council on research project B-Q47U “Infrasonic Vibration Suppression Using Viscoelastic Dynamic Absorber” under grant number 15211215.

References

[1] Asami, T., Sekiguchi, H., 1990, “Fundamental Investigation on Air Damper (2nd Report, Theoretical and Experimental Study),” Trans. Jpn. Soc. Mech. Eng., 56-532, Ser. C, pp.3201-3209.

[2] Asami, T., Moroose, K., Iribe, K., Hosokawa, Y., 1993, “Methods for Designing an Air Damper,” Trans. Jpn. Soc. Mech. Eng., 59-566, Ser. C, pp.2996-3002.

[3] Gatade, Y., Misawa, H., Seto, K., Doi, F., 1996, “Optimal Design of Notch Type Dynamic Absorber,” Prepr. of Jpn. Soc. Mech. Eng., No. 96-5(1), Vol. B, pp.569-572.

[4] Satoh, Y., 1991, “The Reductive Performance of the Dynamic Absorbers and Dynamic Properties of the Viscoelasdc Absorber Elements,” Trans. Jpn. Soc. Mech. Eng., 57-534, Ser. C, pp.446-452 (in Japanese).

[5] Asami, T., Nishihara, O., 1999, “Analytical and Experimental Evaluation of an Air Damped Dynamic Vibration Absorber: Design Optimizations of the Three-Element Type Model,” ASME, Journal of Vibration and Acoustics, 121, pp.334-342.

[6] Anha, N.D., Nguyen, N.X., Hoa, L.T., 2013, “Design of three-element dynamic vibration absorber for damped linear structures,” Journal of Sound and Vibration, 332(19), pp.4482-4495.

[7] Hatada, T., Kobori, T., Ishida, M., Niwa, N., 2000, “Dynamic analysis of structures with Maxwell model,” Earthquake Eng Struct Dynam 29(2), pp.159–76.

[8] Love, J.S., Tait, M.J., 2015, “The peak response distributions of structure–DVA systems with nonlinear damping” Journal of Sound and Vibration, 348(21), pp.329-343.

[9] Krenk, S., 2005, “Frequency Analysis of the Tuned Mass Damper,” ASME J. Appl. Mech., 72(6), pp.936-942.

[10] Bhattacharyya, S., Ghosh, A., Basu, B., 2017, “Nonlinear modeling and validation of air spring effects in a sealed tuned liquid column damper for structural control,” Journal of Sound and Vibration, 410(8), pp.269-286.

[11] Makris, N., Constantinou, M.C., Dargush G.F., 1993, “Analytical model of viscoelastic fluid dampers,” J Struct Eng (ASCE) 119(11), pp.3310–25.

[12] Chen, Y.T., Chai, Y.H., 2011, “Effects of brace stiffness on performance of structures with supplemental Maxwell model-based brace-damper systems,” Earthquake Eng Struct Dynam 40(1), pp.75–92.

[13] Pawlak, Z., Lewandowski, R., 2013, “The continuation method for the eigenvalue problem of structures with viscoelastic dampers,” Computers and Strutures 125, pp.53-61.

[14] Lu, L., Lin, G., Shih, M., 2012, “An experimental study on a generalized Maxwell model for nonlinear viscoelastic dampers used in seismic isolation,” Engineering Structures 34, pp.111-123.

[15] Todkar, R.G., 2011, “Design, development and testing of an air damper to control the resonant response of a SDOF quarter-car suspension system,” Modern Mechanical Engineering 1, pp.84-92.

[16] Lu L., Lin T., Jheng R., Wu H., 2018, “Theoretical and experimental investigation of position-controlled semi-active friction damper for seismic structures,” Journal of Sound and

Vibration, 412(6), pp.184-206.

[17] Wong, W.O., Cheung, Y. L., 2008, “Optimal design of a damped dynamic vibration absorber for vibration control of structure excited by ground motion,” Engineering Structures 30, pp.282–286.

Figure Captions

Fig.1 Air damper model using Maxwell element.

Fig.2 Modeling of structural system by Maxwell-VC DVA.

Fig.3 Air damper model using transformed Voigt element.

Fig.4 Contour chart of $\max|H(U)|$ on $\varsigma_c - \varsigma_m$ plane with design optimal $[\varsigma_c, \varsigma_m]_W$ =[0.22, 0.10], contour minimization $[\varsigma_c, \varsigma_m]_X$ =[0.14, 0.11], design minimization $[\varsigma_c, \varsigma_m]_Y$ =[0.13, 0.112].

Fig.5 $|H(U)|$ comparison of contour optimal W(——), contour minimization Y(- - -) and three-element optimal (— —).

Fig.6 Contour chart of $\min|H(U)|$ at λ_s=3.0 on $\varsigma_c - \varsigma_m$ plane (μ_{Opt} = 0.20, $\gamma_d^{'}$ = 0.8073, $\gamma_m^{'}$ = 8.125).

Fig.7 Comparison of optimal design curve (——) and contour optimal (- - -) on $\max|H(U)|$ contour.

Fig.8 Optimal design curve(- - -) on $\max|H(U_d - U)|$ contour.

Fig.9 $|H(U_d - U)|$ of fixed points minimization at λ_s = 3.

Fig.10 Test platform of Maxwell VC-DVA: air damper, linear slide block system and spectrum analyzer computer system.

Fig.11 Schematic diagram of air damper.

Fig.12 Coulomb damping force $\Im_c$ against θ_c (△ Force test — — Line fit).

Fig.13 Optimal experimental data set of θ_v against θ_c.

Fig.14 Frequency response functions of experimental optimal *We*(——), minimization *Ye*(—— -) and ς_c intercept *Ve*(- - - -).

Fig.15 Variation of $|H(U)|$ along optimal experimental curve.

Fig.16 Comparison of optimal design curve (- - -) and optimal experimental curve(——)

with $[\varsigma_c,\varsigma_m]_V^e$ =[0.395, 0.002], $[\varsigma_c,\varsigma_m]_W^e$ =[0.22, 0.098] and $[\varsigma_c,\varsigma_m]_Y^e$ =[0.13, 0.11].

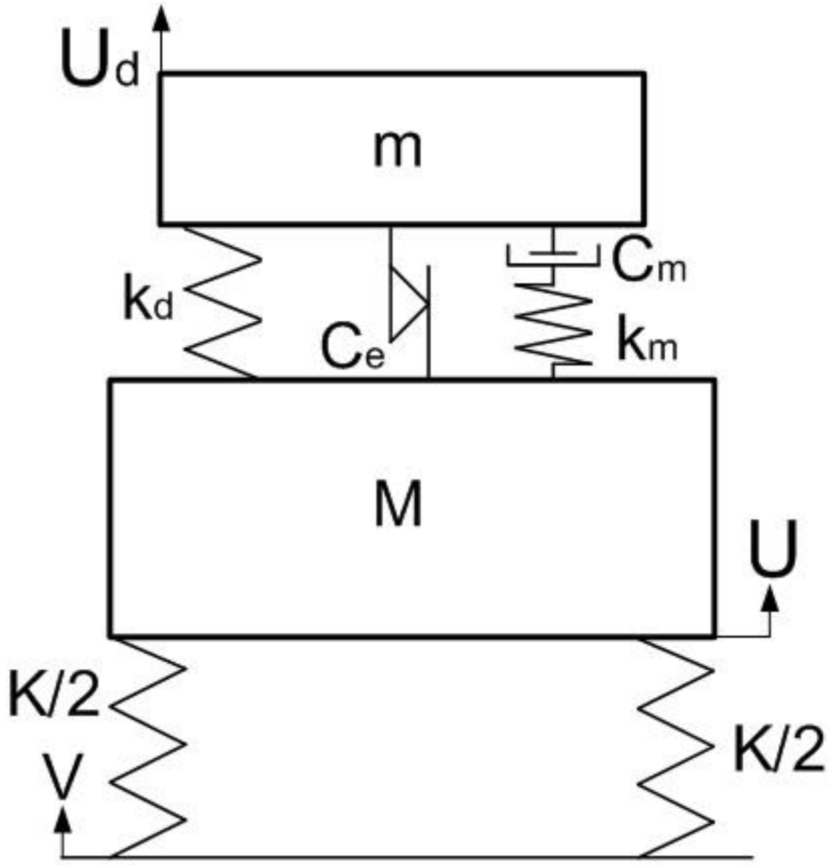

Fig.1 Air damper damped system model using Maxwell element.

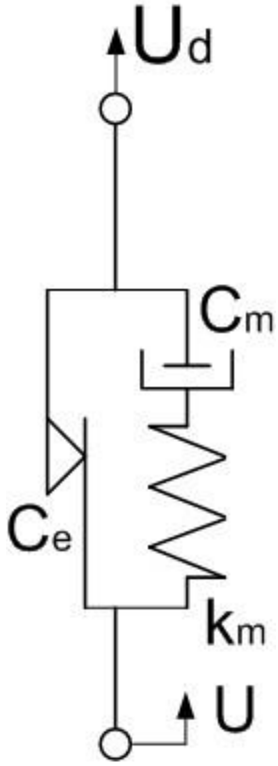

Fig.2 Modeling of structural system by Maxwell-VC DVA.

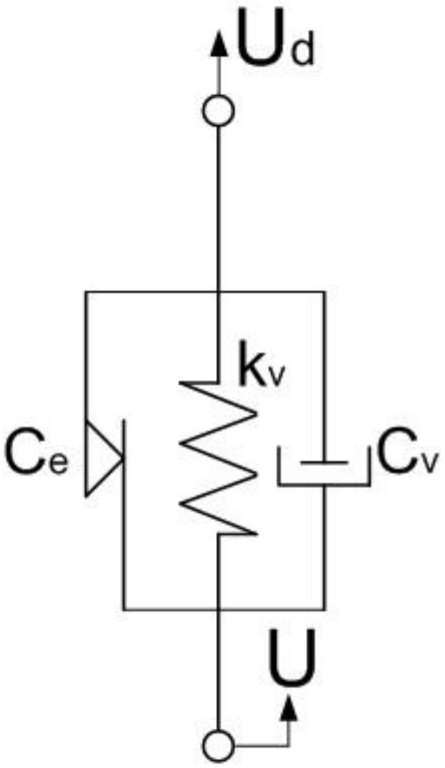

Fig.3 Air damper model using transformed Voigt element.

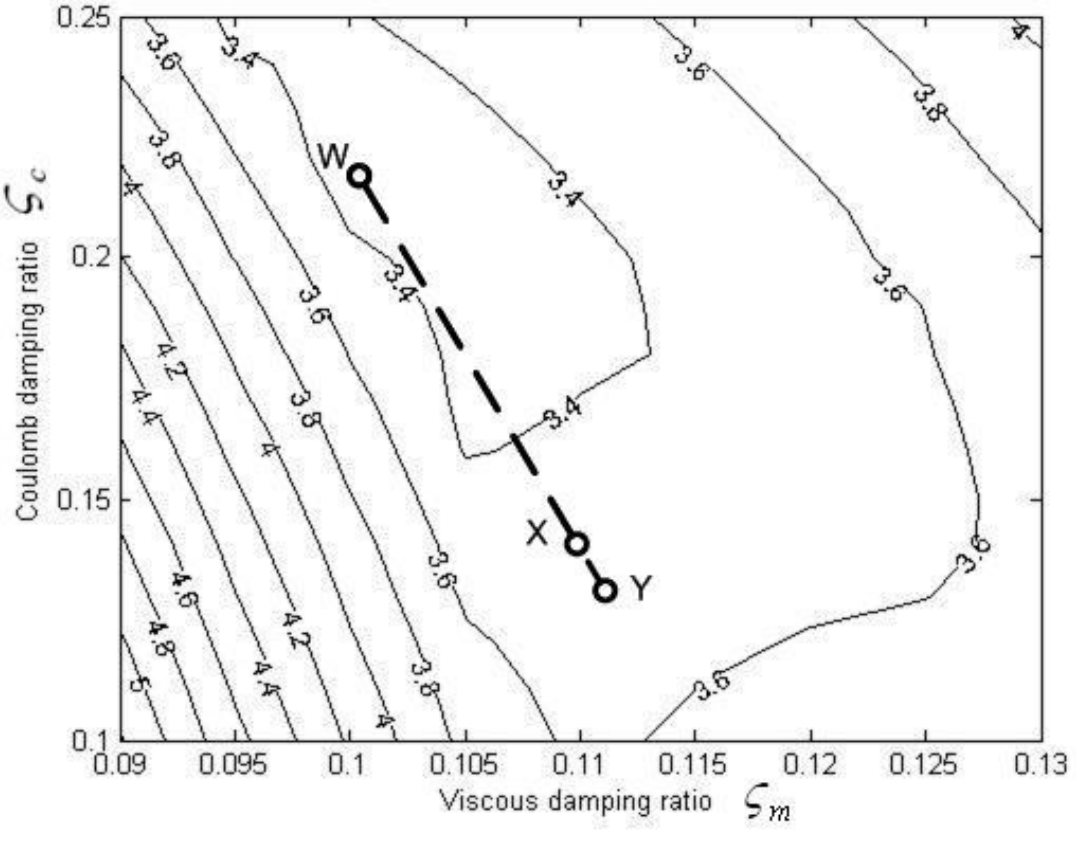

Fig.4 Contour chart of $\max\left|H(U)\right|$ on $\varsigma_c - \varsigma_m$ plane with design optimal $[\varsigma_c, \varsigma_m]_W$ =[0.22, 0.10], contour minimization $[\varsigma_c, \varsigma_m]_X$ =[0.14, 0.11], design minimization $[\varsigma_c, \varsigma_m]_Y$ =[0.13, 0.112].

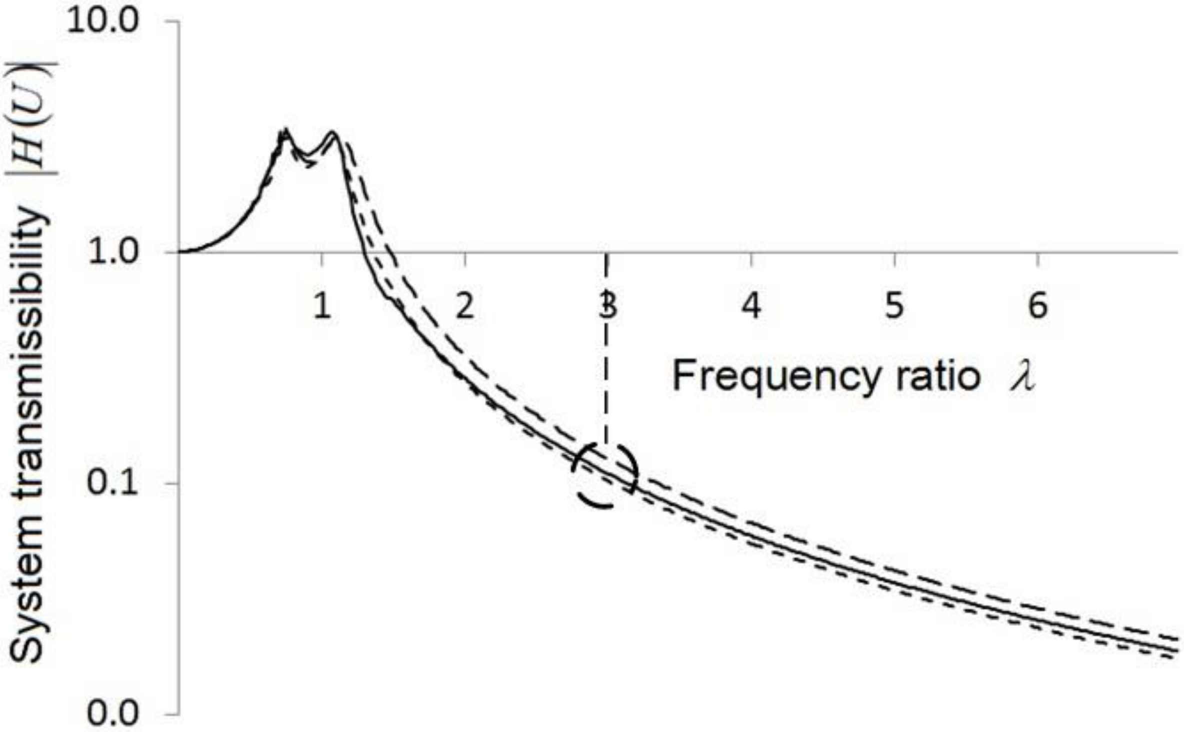

Fig.5 $|H(U)|$ comparison of contour optimal W(——), contour minimization Y(- - -) and three-element optimal[5] (— —).

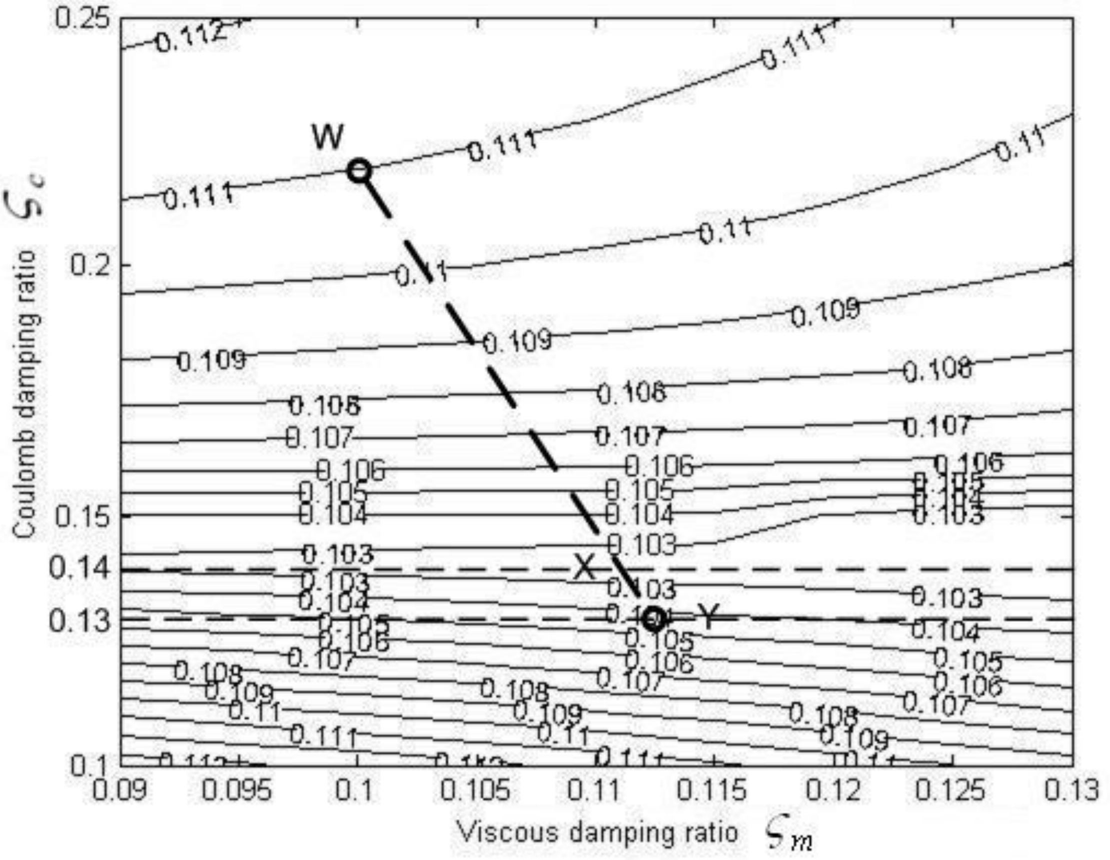

Fig.6 Contour chart of $\min\left|H(U)\right|$ at λ_s=3.0 on $\varsigma_c-\varsigma_m$ plane

(μ_{Opt} = 0.20, γ'_d = 0.8073, γ'_m = 8.125).

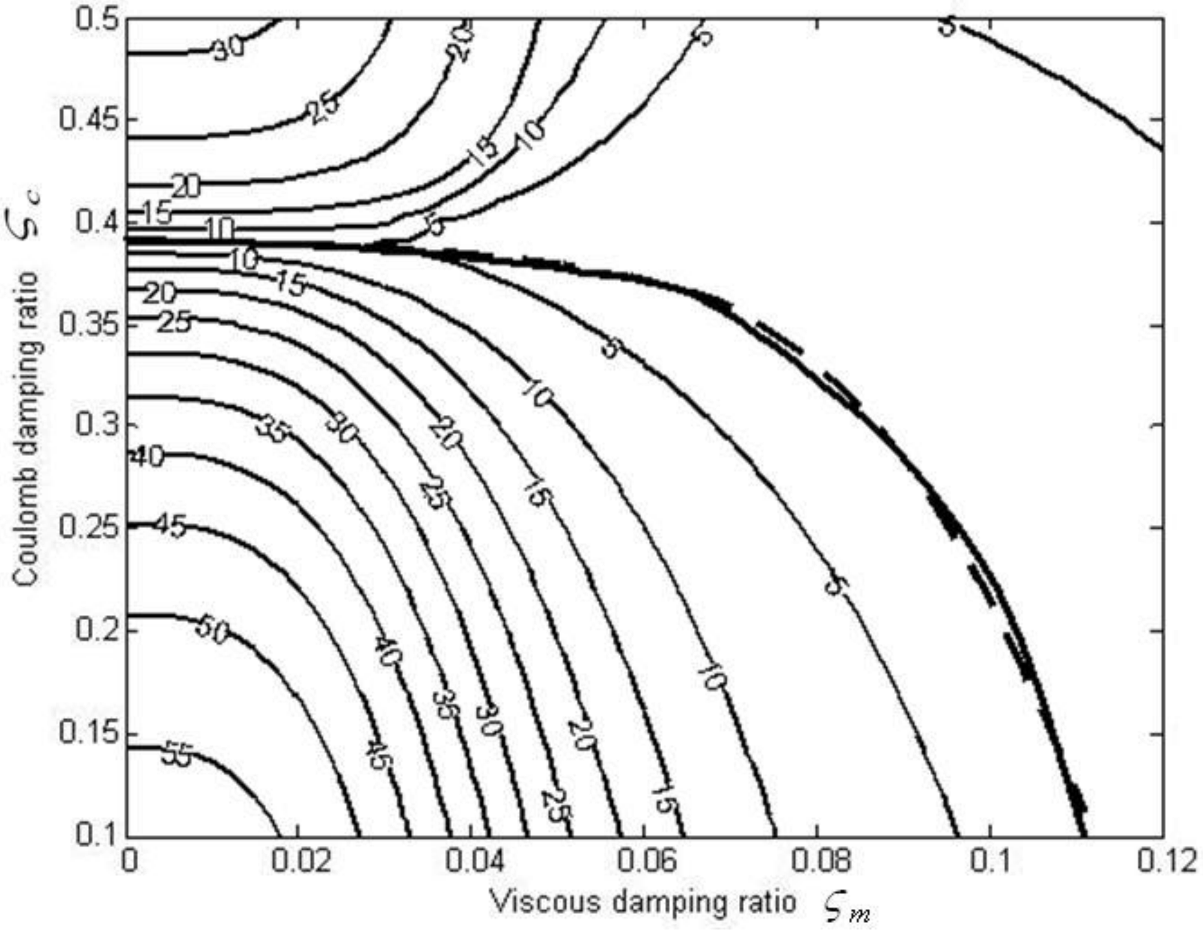

Fig.7 Comparison of design optimal (——) and contour optimal (- - -)

on max$|H(U)|$ contour.

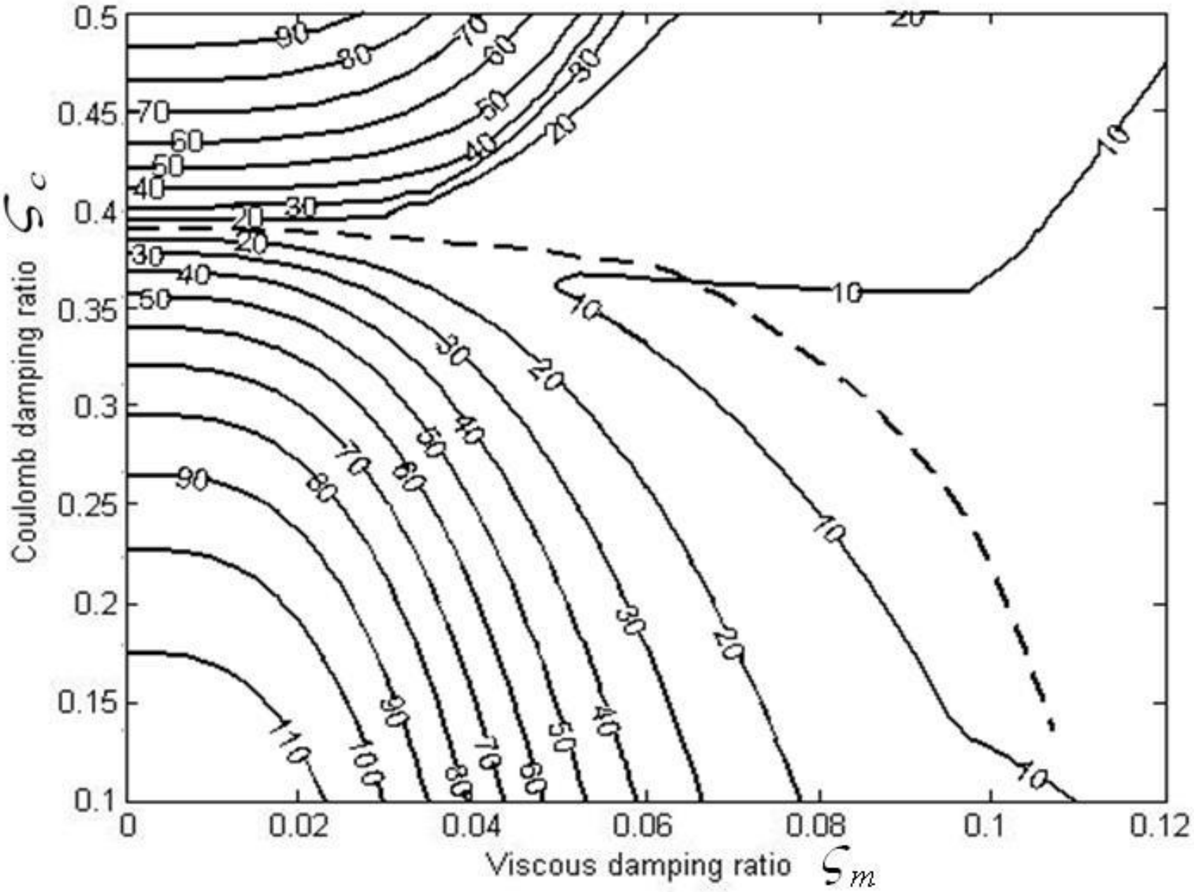

Fig.8 Optimal design curve(− − −) on max$\left|H\left(U_d-U\right)\right|$ contour.

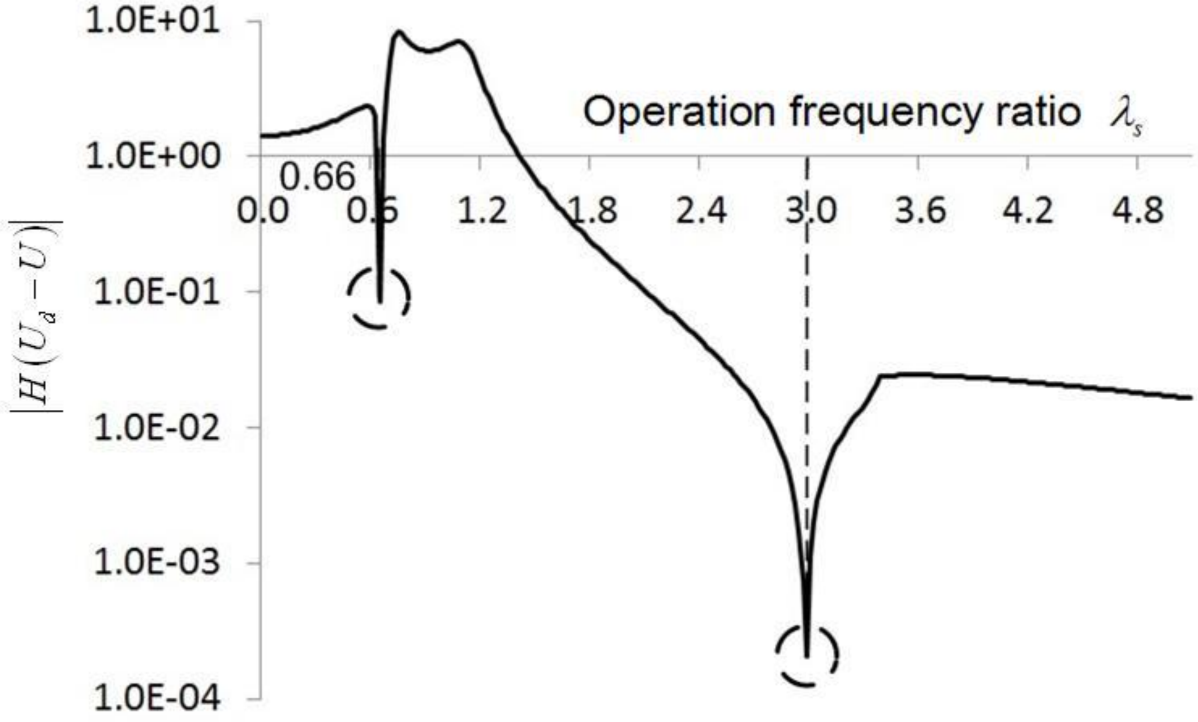

Fig.9 $\left|H\left(U_d - U\right)\right|$ of fixed points minimization at $\lambda_s = 3$.

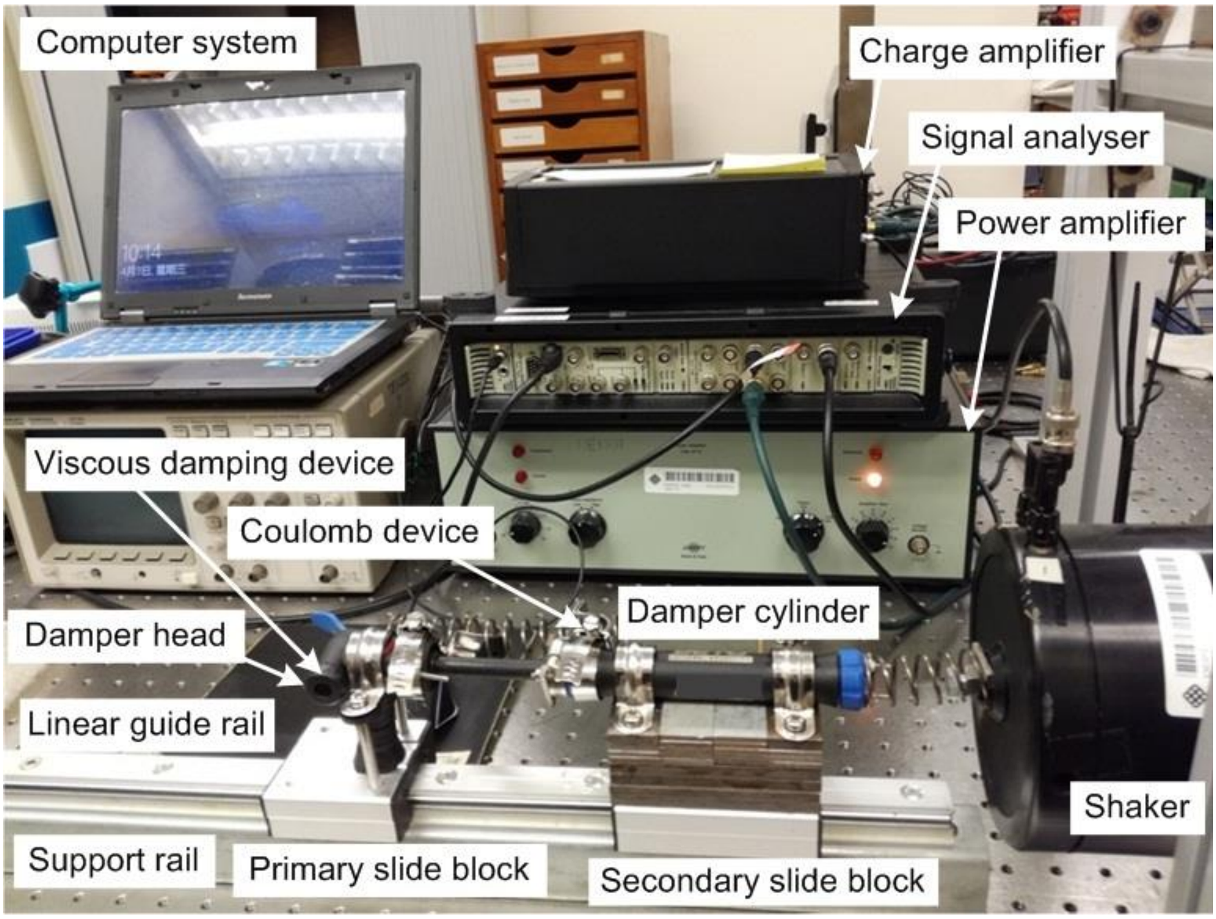

Fig.10 Test platform of Maxwell VC-DVA: air damper, linear slide block system and spectrum analyzer computer system.

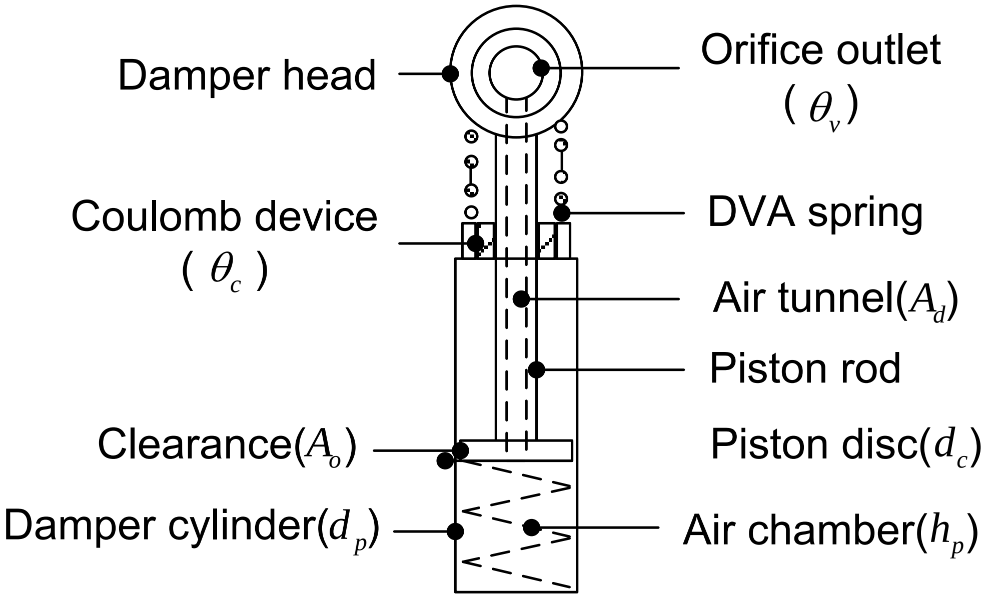

Fig.11 Schematic diagram of air damper.

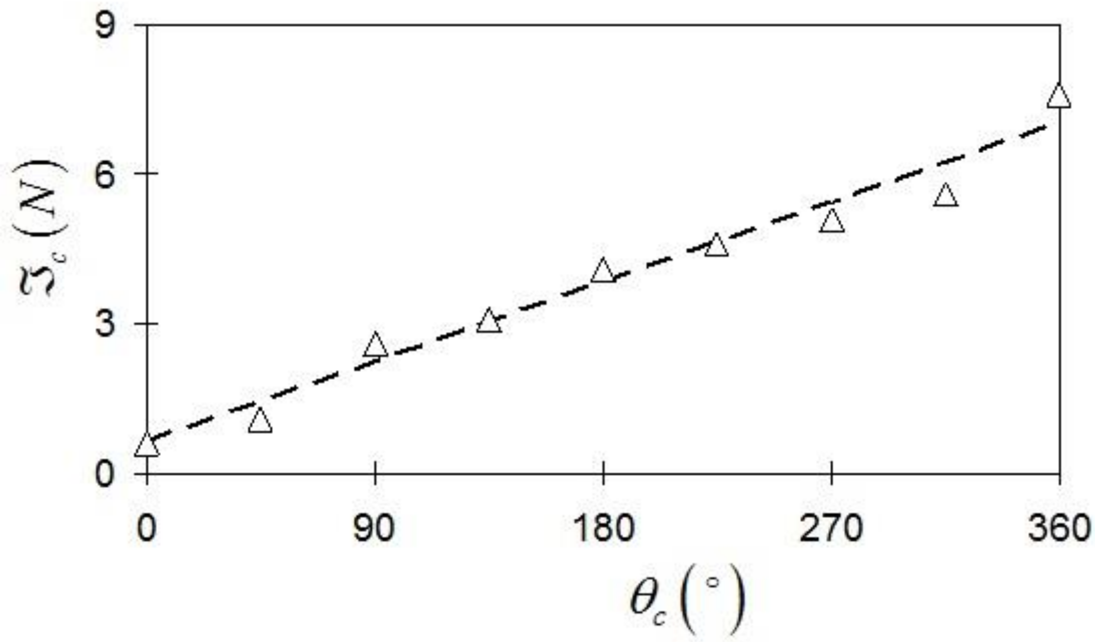

Fig.12 Coulomb damping force $\Im_c$ against θ_c (△ Force test – – Line fit).

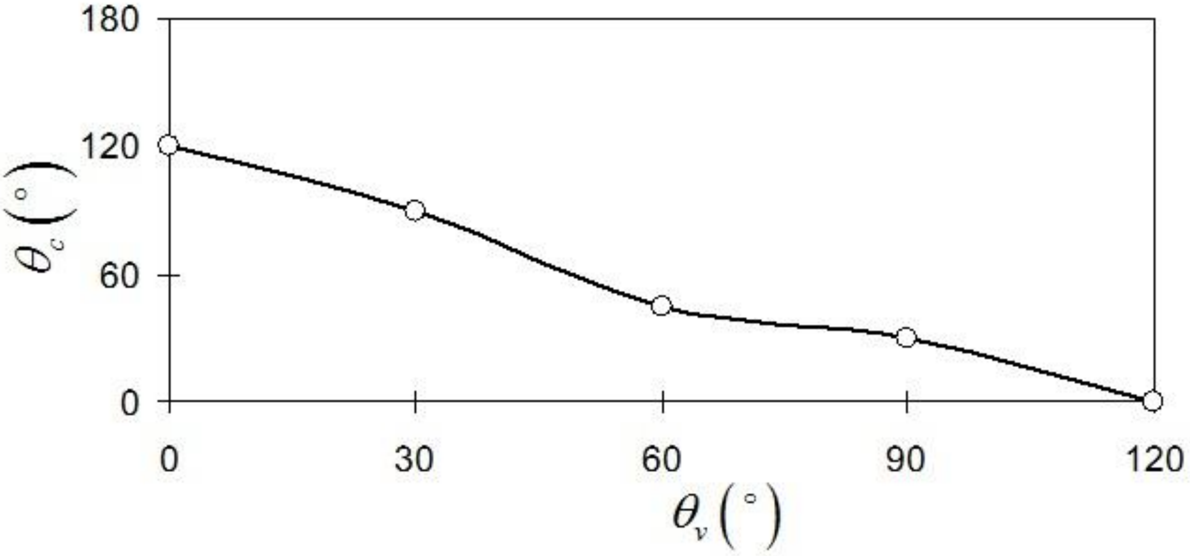

Fig.13 Optimal experimental data set of θ_v against θ_c.

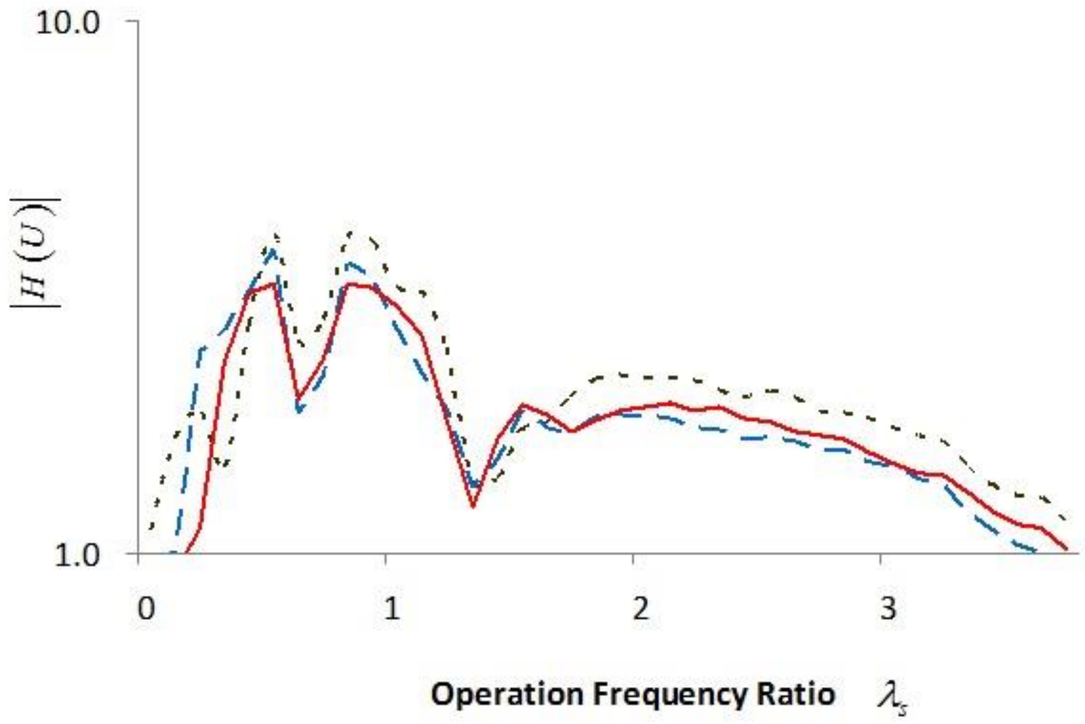

Fig.14 Frequency response functions of experimental optimal *We*(——), minimization *Ye*(— –) and ς_c intercept *Ve*(- - - -).

.

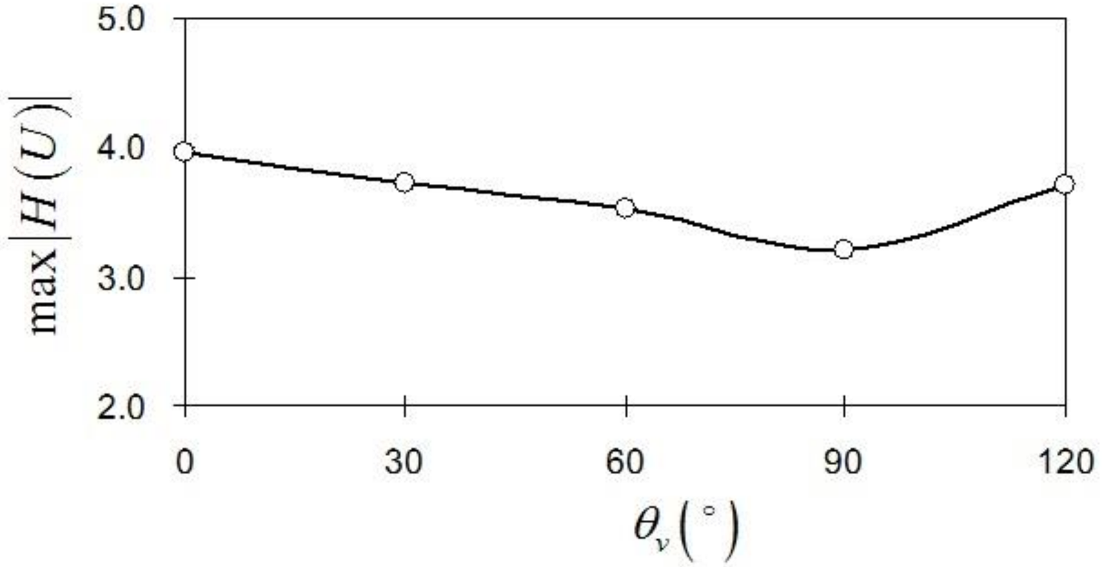

Fig.15 Variation of $\max\left|H(U)\right|$ along optimal experimental curve.

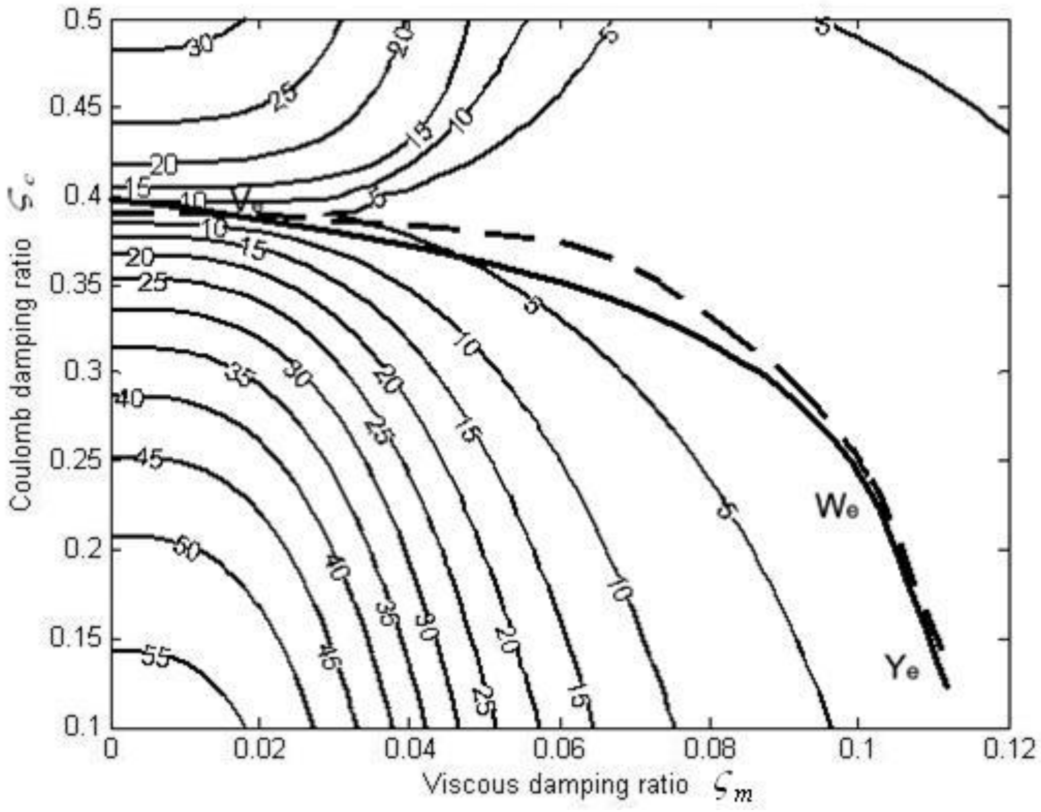

Fig.16 Comparison of optimal design curve (– – –) and optimal experimental curve(——)

with $[\varsigma_c,\varsigma_m]_V^e$ =[0.395, 0.002], $[\varsigma_c,\varsigma_m]_W^e$ =[0.22, 0.098] and $[\varsigma_c,\varsigma_m]_Y^e$ =[0.13, 0.11].